Original Paper

Early View publication on
www.interscience.wiley.com
(issue and page numbers not yet assigned;
citable using Digital Object Identifier – **DOI**)

phys. stat. sol. (b), 1–5 (2006) / **DOI** 10.1002/pssb.200669192

The Kataura plot over broad energy and diameter ranges

Ado Jorio[*, 1], **Paulo T. Araujo**[1], **Stephen K. Doorn**[2], **Shigeo Maruyama**[3], **Helio Chacham**[1], and **Marcos A. Pimenta**[3]

[1] Departamento de Física, Univ. Federal de Minas Gerais, Belo Horizonte, MG, 30123-970, Brazil
[2] Chemistry Division, Los Alamos National Laboratory, Los Alamos, NM 87545, USA
[3] Department of Mechanical Engineering, The University of Tokyo, Tokyo 113-8656, Japan

Received 28 June 2006, revised 24 July 2006, accepted 3 August 2006
Published online 19 September 2006

PACS 71.35.–y, 73.22.–f, 78.30.Na, 78.55.–m, 78.67.Ch

The theoretical plot presenting the optical transition energies for carbon nanotubes as a function of tube diameter was proposed in 1999 and became the most used guide for researchers in the field. This work presents this plot obtained experimentally in a broad range of excitation laser energies (1.26–2.7 eV) and nanotube diameters (0.7–2.3 nm). The results include the poorly studied E_{33}^{S} and E_{44}^{S} optical transitions, and indicate the higher levels are not excitonic, but related to free electron–holes making band-to-band transitions.

1 Introduction

The nowadays baptized "Kataura plot" [1], plotting the optical transition energies for any single-wall carbon nanotube isomer as a function of tube diameter, became very popular in the carbon nanotube field because the optical techniques have been readily used to study and characterize carbon nanotube samples, from its synthesis up to the most advanced manipulation procedure related to device fabrication. However, since 1999, researchers try to build the Kataura plot by joining many pieces of information, just like trying to solve a puzzle. The theoretical background to predict and extrapolate the results for non-measured carbon nanotubes is not yet fully established, due to the difficulty in determining the electron–electron and electron–hole interactions in this quasi-one dimensional material [2–6]. Different samples with different tube diameter distributions, under different environmental conditions have been analyzed [7]. The results are obtained by using different techniques under different experimental conditions. This procedure has generated a fragmented and, consequently, a hard to trust guide for optical characterization of carbon nanotube samples. This work presents, in Fig. 1, the Kataura plot that represents the optical properties of carbon nanotubes in a broad range of tube diameters, with well-controlled experimental conditions all over the usually important optical energy range.

To study the photophysics of carbon nanotubes, the well-established, readily available and readily applied optical techniques are the optical absorption, the resonance Raman spectroscopy and the photoluminescence excitation [7]. To generate the Kataura plot, optical absorption [1] has a serious limitation for only measuring the absorption energy, and it cannot be used to differentiate carbon nanotubes with similar optical transition energies. Photoluminescence cannot be used to obtain the optical transition energy for metallic tubes, it is usually absent for zigzag (n, 0) SWNTs [8], and in the case of semiconducting tubes, it is limited to isolated nanotubes, either suspended in liquid solution [8] or by silicon

* Corresponding author: e-mail: adojorio@fisica.ufmg.br

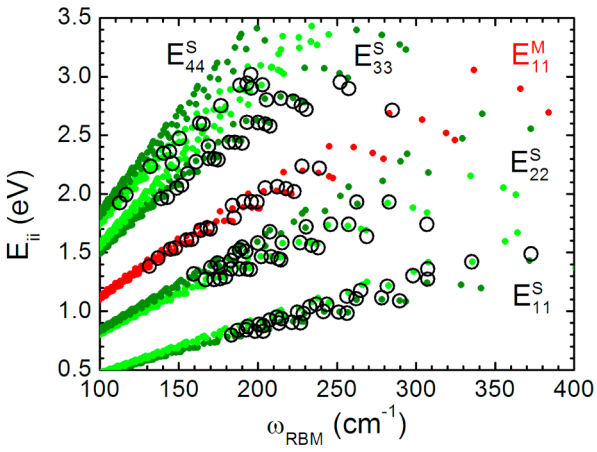

Fig. 1 (online colour at: www.pss-b.com) Optical transition energies E_{ii} for carbon nanotubes as a function of the radial breathing mode (RBM) frequency (ω_{RBM}). Red, green and olive bullets stand for carbon nanotubes with $(2n + m)$ mod 3 = 0 (metallic), 1 and 2 (semiconducting), respectively. The bullets are obtained by extrapolation of the experimental data (open circles) from resonance Raman spectroscopy [13].

pillars [9]. The resonance Raman spectroscopy, when performed with a quasi-continuous set of excitation laser lines, can be used to build a two-dimensional plot that represents the Kataura plot as it is, and with no experimental or physical limitation.

2 Experimental details

The sample used for the experiment is the vertically aligned single-wall carbon nanotubes, grown by the chemical vapor deposition method from alcohol [10]. The alcohol sample presents carbon nanotubes covering most of the diameter range of usual interest (0.7–2.3 nm). Their impurity content is very low and they are here measured as grown – no chemical/physical manipulation procedure. Because these nanotubes are grown vertically aligned from a substrate, they do not show considerable bundling or heating effects under laser irradiation [11, 12]. Two triple-monochromator Raman spectrometers, equipped with coupled charge device (CCD) detectors, were used to perform the measurements – a Dilor XY for experiments in the visible range, and a SPEX in the near infrared range. Back-scattering configuration was used. The 95 different excitation come from an ArKr laser, a Ti:Sapphire laser and a Dye laser pumped by a 6 W Ar laser. A single-monochromator was used to filter the incident excitation laser line.

Intensity analysis shows that the higher the energy level (i.e. the higher the i sub-index in E_{ii}), the lower and broader the resonance profile. The maximum intensity for the E_{22}^{S} resonance profile of a semiconducting nanotube is at least one order of magnitude higher than the maximum intensity for the resonance profile of the E_{33}^{S} level. Important trends that are observed in the resonance Raman spectra are the geometric patterns related to carbon nanotubes of similar diameters, but varying the chiral angles from $\theta = 30°$ (armchair nanotubes) to $\theta = 0$ (zigzag nanotubes). These families of tubes can be indexed by the carbon nanotube (n, m) indices defining (d_t, θ), since they have $2n + m =$ constant, as shown by the sub-branches inside each E_{ii} in Fig. 1. The Raman cross-section for carbon nanotube with $\theta \to 0$ is always about one order of magnitude stronger than the Raman cross-section for carbon nanotube with $\theta \to 30°$.

3 Results and discussions

Figure 1 gives the optical transition energies E_{ii} for over 200 SWNTs as a function of the radial breathing mode frequency (ω_{RBM}). The open circles are obtained experimentally [13]. The colored bullets give the $E_{ii} = \sum_l \alpha_l (p/d_t)^l + \beta_p \cos(3\theta)/d_t^2$ for the excitonic levels E_{11}^{S}, E_{22}^{S} and E_{11}^{M}. In the polynomal expansion on (p/dt), terms up to $l = 5$ are need for a good description of the observed E_{ii}, and the experimentally obtained values for α_l and β_p are given in Ref. [13]. The d_t and θ are the tube diameter and chiral angle, and p = 1, 2, 3, 4, 5 for E_{11}^{S}, E_{22}^{S}, E_{11}^{M}, E_{33}^{S} and E_{44}^{S}, respectively. Our result suggests that the E_{33}^{S} and E_{44}^{S}

are not excitonic, but band-to-band transitions, with energies given by $E_{ii} + \Delta E$. The ΔE is the experimentally obtained diameter dependence of the exciton binding energy [13]. The diameter d_t is related to ω_{RBM} by the relation $\omega_{RBM}\,(\mathrm{cm}^{-1}) = 217.8/d_t\,(\mathrm{nm}) + 15.7$.

In a first approximation, the electronic transition energies E_{ii} for carbon nanotubes exhibit both a diameter (d_t) and a relatively smaller chiral angle (θ) dependence, given by

$$E_{ii} = \alpha/d_t + \beta_p \cos(3\theta)/d_t^2 \,. \tag{1}$$

The β_p-factor measures the chiral angle dependence, and it is different for each E_{ii} subband, increasing for larger i due to the increase of the trigonal warping effect [14]. For semiconducting carbon nanotubes, β_p also depends on $(2n + m) \bmod 3 = 1$ or 2, which defines type 1 vs. type 2 semiconducting carbon nanotubes, that exhibit opposite chiral angle dependence [14]. The chirality dependent factor in Eq. (1) shrinks the points related to a same E_{ii} level into one single diameter dependent curve.

The α in Eq. (1) can be determined by the linear dispersion relation of π-electrons in graphite using the tight-binding method [14], considering only first-neighbor interactions, given by $\alpha = (2/3)\gamma_0 a_{C\text{–}C} p$. The factor p = 1, 2, 3, 4 and 5 stands for E^{S}_{11}, E^{S}_{22}, E^{M}_{11}, E^{S}_{33} and E^{S}_{44}, respectively. The p-factor is expected to collapse all the E_{ii} sub-bands into one curve when plotting E_{ii} as a function of p/d_t. For example, while the first optical level $E^{S}_{11} = 1$ eV for a 1 nm diameter semiconducting tube, the second optical level $E^{S}_{22} = 1$ eV for a 2 nm diameter tube. The tight-binding overlap integral $\gamma_0 = 2.9$ eV has been shown to be the best value to describe the optical transition energies of carbon nanotubes with this simple tight-binding method [14]. Figure 2 shows how the experimental points measured in this work deviates from Eq. (1), the deviations going to zero on average. The data points deviates from zero due to the non-linearity in the dispersion relation for π-electrons (more important for high-energy levels), due to the effects of tube curvature [15, 16], and due to many-body (electron–electron and electron–hole) interactions [2–5].

For a better description of the electronic structure within the tight binding method one has to consider an extended non-orthogonal tight-binding model that fully considers the effects of curvature (σ–π hybridization and asymmetric bond angles and lengths variations) [15, 16], plus the blue-shift correction due to many-body effects [5, 15, 17]. In Fig. 3 we show how the experimental optical transition energies deviate from the extended non-orthogonal tight-binding model [15]. These deviations correspond to corrections ΔE^{mb} that have to be performed in the extended non-orthogonal tight-binding model to account for the many-body effects.

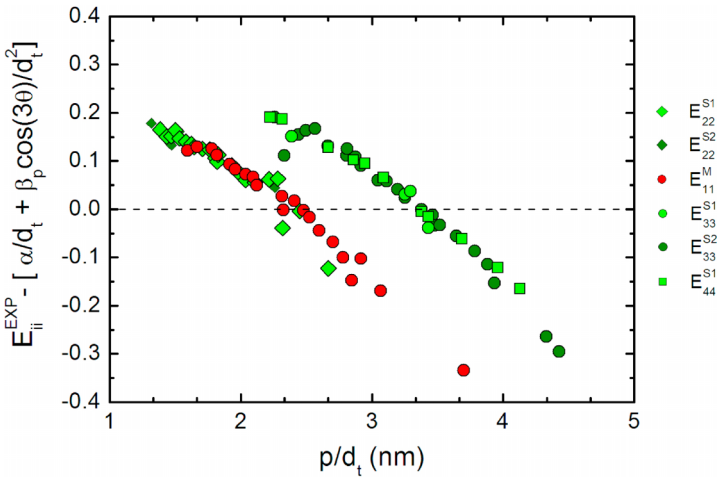

Fig. 2 (online colour at: www.pss-b.com) Deviation of the experimentally obtained transition energies from Eq. (1). Different symbols (see legend) stand for different E_{ii} levels and semiconducting type 1 (S1) and type 2 (S2), as defined by the mod values in the caption to Fig. 1.

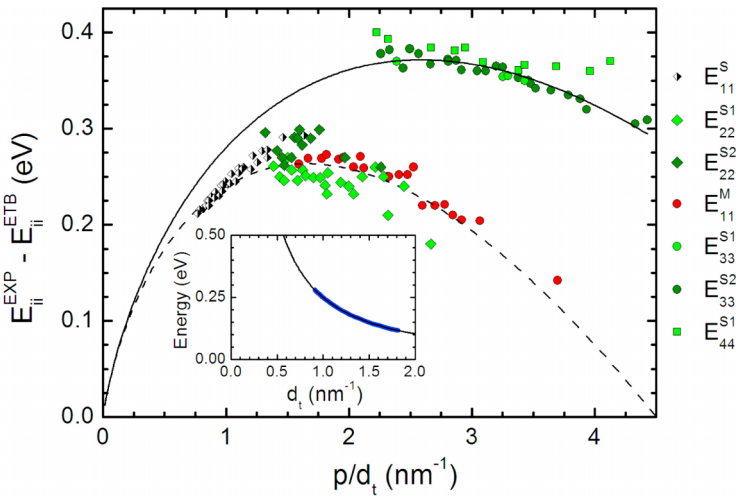

Fig. 3 (online colour at: www.pss-b.com) Deviation of the experimentally obtained optical transition energies from the values predicted by the extended tight binding model [15]. The dashed line shows a fit to E_{11}^{S}, E_{22}^{S} and E_{11}^{M} using Eq. (2). The solid line is obtained by summing a $\Delta E = \gamma/d_t$ in the dashed line to fit E_{33}^{S} and E_{44}^{S}. The inset shows the difference betwen the two scaling laws, i.e. ΔE.

The electron–electron and electron–hole (many-body) interactions are expected to be very strong in one-dimensional systems due to the spatial confinement [2–5]. Both electron–electron and electron–hole long range one-dimensional coulomb interactions (with length scales larger than tube circumference) are predicted to strongly depend on the inverse tube diameter, competing and nearly cancelling each other [5]. As a result of this cancellation, the observed optical transitions in carbon nanotubes are dominated by short range two-dimensional graphene self-energy effects, leading to a logarithmic correction to the electronic self-energy of the first (E_{11}) and second (E_{22}) related levels, and marginal Fermi liquid behaviour [5]. Therefore, the many-body corrections for E_{11}^{S}, E_{22}^{S} have been described by a scaling law established in the literature [5, 17]:

$$\Delta E^{mb} = \gamma_0 a_{C-C}(g/4)\,(2p/3d_t)\,\log\,[2\Lambda(2p/3d_t)]\,, \qquad (2)$$

where g is a dimensionless parameter characterizing the Coulomb interaction and Λ is an ultraviolet cutoff of order of the inverse lattice constant [5]. In Fig. 3 the data related with E_{11}^{S}, E_{22}^{S} and E_{11}^{M} transitions in our sample follow the scaling law in Eq. (2). The best fit to our E_{11}^{S}, E_{22}^{S} and E_{11}^{M} data (dashed line in Fig. 3) is given by $\gamma_0 a_{C-C}(g/4) = 0.55$ eV nm and $\Lambda = 1.50$ nm^{-1} [17]. The E_{33}^{S} and E_{44}^{S} transitions do not follow the same scaling law, and the deviation from the extended tight binding method can be fit by summing a $\Delta E = \gamma/d_t$ dependence to the many-body corrections ΔE^{mb} in Eq. (1). The E_{33}^{S} and E_{44}^{S} are, therefore, blue-shifted from the excitonic scaling law, and the blueshift goes with inverse diameter, like the exciton binding energy [2–5]. This result suggests that the E_{33}^{S} and E_{44}^{S} are not excitonic in nature, but rather related to free electron–hole pairs making band-to-band transitions [13].

One could argue that the higher energy levels (E_{33}^{S}, E_{44}^{S}) could deviate from the scaling developed for lower energy levels (E_{11}^{S}, E_{22}^{S}) because they are in a different energy range. The many-body corrections scaling proposed by Kane and Mele [5] have an energy cutoff, and higher energy levels could deviate from the scaling developed for lower energy levels. However, this is not the case for the present work, since the established scaling for E_{11}^{S}, E_{22}^{S} is based on experimental measurements that go up to 2.7 eV [5, 8], while the experimental results for E_{33}^{S} measured in this work go down to 1.9 eV [13].

It is interesting to comment on the results from metallic tubes. Metallic materials are expected to exhibit very different many-body effects when compared with semiconducting materials, because of screening by free electrons in metals. Usually metallic systems do not exhibit real excitons, but rather

excitonic resonances, since they can always decay into the continuum of states. The observation of excitons in carbon nanotubes has been explained as an interesting symmetry related effect [2]. The possibility for a symmetry based explanation for the observation of two different scaling laws observed here has to be addressed theoretically and experimentally. The single scaling law for the E_{11}^{S}, E_{22}^{S} and E_{11}^{M} levels is an interesting phenomena of 1D systems, probable due to the near cancellation of the repulsive electron–electron versus attractive electron–hole interactions.

Finally, the results here should be compared to published results. The simple linear functional we obtain relating the radial breathing mode frequency and the tube diameter is in agreement with well established results for lower diameter tubes [8, 11, 12, 18]. However, recent work proposes a non-linear relation to account for the radial breathing mode frequency of larger diameter tubes [20]. In our experimental data, that includes nanotubes with diameters up to 2.3 nm, the simple linear scale describes the data within experimental precision. Understanding the discrepancies between the two sets of data is an open issue. With respect to the optical transition energies, our results are in very good agreement with all published results for E_{22}^{S} and E_{11}^{M} [8, 11, 12, 18] (E_{11}^{S} is not measured here). Recently E_{33}^{S} and E_{44}^{S} have been obtained for a few carbon nanotubes by Rayleigh scattering [20]. Our results for semiconducting carbon nanotubes are also in excellent agreement with values obtained by Rayleigh scattering. For the metallic tubes there is a considerable discrepancy (~70 meV) between the results obtained with resonance Raman (this work) and Rayleigh scattering [20]. Understanding the discrepancies between these two sets of data for metallic tubes is another open issue.

Acknowledgement A.J. acknowledges the IWEPNM organizing committee for the invitation and financial support to attend the IWEPNM in 2006. The Brazilian authors acknowledge financial support from FAPEMIG and CNPq. SKD acknowledges support from LANL Integrated Spectroscopy Lab. and LANL LDRD program.

References

[1] H. Kataura et al., Synth. Met. **103**, 2555 (1999).
[2] C. D. Spataru et al., Phys. Rev. Lett. **92**, 077402 (2004).
[3] E. Chang et al., Phys. Rev. Lett. **92**, 196401 (2004).
[4] V. Perebeinos, J. Tersoff, and Ph. Avouris, Phys. Rev. Lett. **92**, 257402 (2004).
[5] C. L. Kane and E. J. Mele, Phys. Rev. Lett. **93**, 197402 (2004).
[6] F. Wang et al., Science **308**, 838 (2005).
[7] A. Jorio et al., MRS Bull. **29**, 276 (2004).
[8] S. M. Bachilo et al., Science **298**, 2361 (2002).
[9] J. Lefebvre, Y. Homma, and P. Finnie, Phys. Rev. Lett. **90**, 217401 (2003).
[10] S. Maruyama et al., New J. Phys. **5**, 149 (2003).
[11] C. Fantini et al., Phys. Rev. Lett. **93**, 147406 (2004).
[12] S. K. Doorn et al., Appl. Phys. A **78**, 1147 (2004).
[13] P. T. Araujo et al., submitted.
[14] R. Saito, G. Dresselhaus, and M. S. Dresselhaus, Physical Properties of Carbon Nanotubes (Imperial College Press, London, 1998).
[15] Ge. G. Samsonidze et al., Appl. Phys. Lett. **85**(23), 5703 (2004).
[16] V. N. Popov and L. Henrad, Phys. Rev. B **70**, 115407 (2004).
[17] A. Jorio et al., R. Phys. Rev. B **71**, 075401 (2005).
[18] H. Telg et al., Phys. Rev. Lett. **93**, 177401 (2004).
[19] J. C. Meyer et al., Phys. Rev. Lett. **95**, 217401 (2005).
[20] M. Y. Sfeir et al., Science **312**, 554 (2006).

